JOURNAL OF SPACECRAFT AND ROCKETS
Vol. 32, No. 6, November–December 1995

Analysis of Laminar Near-Wake Hypersonic Flows

F. Grasso* and C. Pettinelli†
University of Rome "La Sapienza," 00184 Rome, Italy

An analysis of laminar hypersonic near-wake flows is presented. The influence of nose bluntness and Mach and Reynolds numbers on the flowfield has been investigated, and the effects on the structure of the recirculation wake have been determined. Analytical correlations for characterizing the near-wake behavior with regard to compressibility effects, extent of upstream influence, separation location, and near-wake aspect ratio have been established by means of numerical simulations and theoretical considerations. In particular the properties of the near wake are found to depend on the local Reynolds number along the recirculation dividing streamline: the base flow changes from a diffusion- to a convection-dominated wake structure depending on the maximum value of the dividing-streamline Reynolds number. For a nearly inviscid recirculation a supersonic reverse flow occurs, with the formation of a secondary recirculation and a reverse-flow standing shock in the vicinity of the rear stagnation point. The upstream influence and the separation location have been shown to depend on the thickness of the subsonic boundary layer as well as the dividing streamline Reynolds number. Some of the conclusions have been validated by comparison with ground-test experimental data.

Nomenclature

b	= half base height; constant
E	= total energy
ℓ_w	= extent of recirculation region
M	= Mach number
p	= pressure
p_0	= total pressure
$\boldsymbol{R}$	= residual
Re	= Reynolds number
R_N/b	= ratio of nose radius to base height
s	= curvilinear abscissa
T	= temperature
T_w	= wall temperature
$\boldsymbol{u}$	= velocity vector
u	= velocity modulus
$\boldsymbol{W}$	= vector of convervative unknowns
γ	= specific heat ratio
$\Delta\ell$	= upstream influence from corner
Δs	= separation distance from corner
δ_s	= thickness of subsonic boundary layer
δ_w	= wake neck thickness
μ	= laminar viscosity coefficient
ρ	= density
$\boldsymbol{\sigma}$	= stress tensor
τ	= wall shear stress
$\boldsymbol{\omega}$	= vorticity vector
ω	= vorticity
ω_w	= wall vorticity

Subscripts

ax	= wake centerline
b	= base
ds	= dividing streamline
e	= edge of mixing layer
sh	= edge of the boundary layer at the shoulder
0	= total; stagnation
∞	= freestream

Received Feb. 22, 1995; revision received June 19, 1995; accepted for publication July 4, 1995.

*Associate Professor, Department of Mechanics and Aeronautics, Via Eudossiana, 18. Member AIAA.

†Graduate Student, Department of Mechanics and Aeronautics, Via Eudossiana, 18.

Introduction

THE study of high-speed (supersonic and hypersonic) wakes has lately gained new interest, due to the development of a whole new class of space vehicles that exploit aerodynamic forces for aerobraking, thus allowing significant fuel savings. Aerobraking is a key element of the aeroassisted orbit transfer vehicles (AOTVs), which are conceived for orbital maneuvers. These vehicles have blunted umbrella-like shapes to generate the very large wave drag needed for aerobraking. The payload is generally located right behind the shield, and understanding of the base flowfield is important to prevent large heat transfer, which can be caused by impinging shear layers and radiation from the shoulder region. The understanding of near-wake flows behind re-entry capsules, missiles, rockets, etc., can also help to improve the stability and the aerodynamic performances of these vehicles.

Figure 1 shows a sketch of a typical flowfield. In the forebody region the fluid strongly decelerates through the bow shock (b), and high pressure, temperature, and density are generated. Depending upon the cruise speed and the altitude, chemical reactions, ionization, and relaxation phenomena may occur. At the shoulder, the flow turns and expands rapidly (e), and the boundary layer detaches, forming a free shear layer (s) that separates the inner recirculation region behind the base from the outer flowfield. The latter is recompressed and turned back to freestream direction, first by the so-called lip shock (l), and further downstream by the recompression shock (r). At the end of the recirculation, past the neck (n), the shear layer develops in the wake trail (t), which is often turbulent and unsteady.

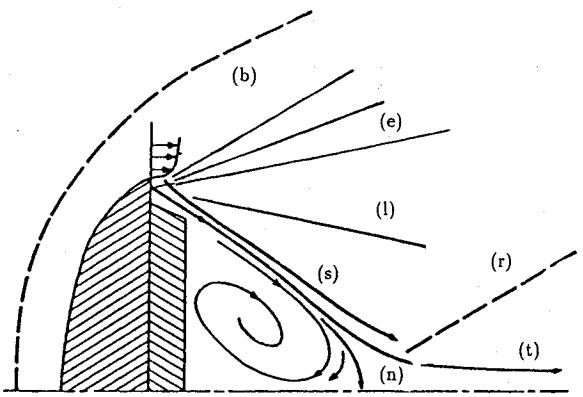

Fig. 1 Sketch of near-wake flow: bow shock (b), expansion (e), free shear layer (s), lip shock (l), recompression shock (r), wake neck (n), and wake trail (t).

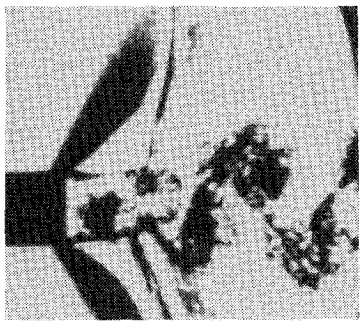

a) $M = 0.925$

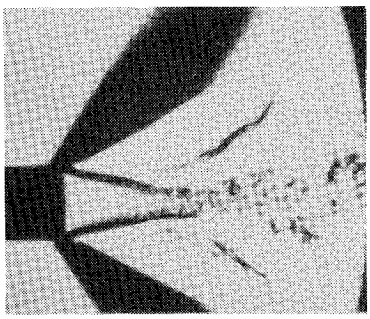

b) $M = 1.00$

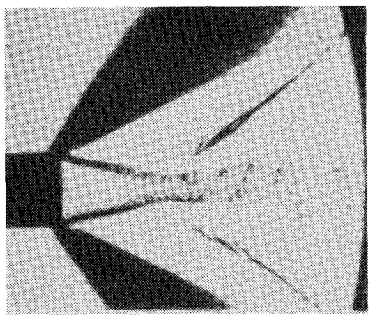

c) $M = 1.05$

Fig. 2 Base flow behind a slender two-dimensional body at transonic speed (from Ref. 2, copyright © 1965, AIAA; reprinted with permission).

For an incompressible flow past a circular cylinder at very low Reynolds number Re, the base flow is laminar and steady, and the extent of the recirculation bubble increases with the Re. As Re reaches about 30–60, instabilities occur in the far wake, and the location of vortex shedding moves towards the shoulder as the Reynolds number is further increased. For $150 \leq Re \leq 10^4$, turbulence first appears in the far wake, and the transition moves upstream along the free shear layer as Re increases. Finally, at $Re \sim 10^5$, transition occurs on the body surface.[1] In general, low-Mach-number and high-Reynolds-number wakes are turbulent and unsteady.

In the compressible case the high Mach number seems to play an important role for stability: stable recirculation regions exist in the supersonic regime at high Re that differ from the subsonic case mainly in the suppression of vortex shedding. Figure 2, taken from Ref. 2, confirms this point; indeed, it shows that the instability in the near wake dies out when the Mach number at the shoulder, (M_{sh}) becomes greater than one. However, the instability does not completely disappear, but remains confined to a thin region along the axis, starting at the point where the two shear layers meet. A further increase in M_{sh} does not produce any qualitative change in the near wake.[2] Experimental ground-test investigations for AOTV configurations have also shown some unsteadiness arising at the wake neck at moderate hypersonic speed[3]; however, the near-wake field appears to be steady. Then, theoretically, one can assume that steady solutions for the near wake exist both for subsonic and supersonic flows, but that only those for $M > 1$ are stable.

In the sixties a variety of experimental and theoretical work on hypersonic wakes was performed.[4–8] Most of the early solutions were obtained by using the method of characteristics, and assuming an experimentally determined shape of the dividing streamline to define the appropriate computational boundary. The recirculation bubble was generally assumed to be a constant-pressure dead-air region that acts as a constant-pressure boundary for the outer flow. The core of the recirculation region was assumed to be dominated by viscous effects, and the outer region was generally assumed to be inviscid. In spite of the simplifying assumptions and the fact that most of the early methods had to rely extensively on experimentally derived parameters, a number of important wake features were established (at least qualitatively). In particular, the influence of the Mach and Reynolds numbers on the base pressure and recirculation length was assessed for several geometrical configurations.[1]

By assuming incompressible behavior of the recirculation region, Weiss[9] has shown that the maximum Reynolds number along the dividing streamline (the so-called dividing-streamline Reynolds number Re_{ds}) is a very important parameter for characterizing the structure of the near wake; moreover, a Stokes-like recirculation region is present for $Re_{ds} \leq 100$ (i.e., diffusion-dominated). Hama[10] experimentally investigated the details of separation from sharp corners, focusing on the formation of the lip shock, and has shown that separation does not occur exactly at the corner, but on the base at a distance from the corner that increases with decreasing Re. Reference 11 has suggested an inviscid wave interaction mechanism that could strengthen the lip shock for sharp corners. It is important to stress, that, for a given base geometry and freestream conditions, the structure of the near wake is also strongly affected by the geometry of the forebody.

The first Navier–Stokes finite difference computations of the near wake have been reported in Ref. 12, fully confirming the observation of Ref. 10 regarding the mechanism of separation. Since the publishing of Ref. 12, a lot of progress in numerical methods and computer performance has been made, and base-flow computations are achieving good predictive capability.

Recently, a large number of numerical simulations of fore- and afterbody flows have been performed for aerobraking configurations. References 13 and 14 use a nonequilibrium reacting-gas model and characterize the complexity of flow interactions in the base region. At high Mach number, the highly dissociated gas (flowing from the forebody) nearly freezes through the expansion at the shoulder. Further downstream the low level of postexpansion pressure inhibits the gas from reaching its equilibrium, and the gas in the base region remains frozen at conditions out of equilibrium (both chemically and thermally). The temperature increases in the wake, reaching very high values, with a maximum in the area where the shear layers meet. The results of Refs. 13 and 14 show good agreement on the forebody, together with the differences in the base region that are likely due to grid inaccuracy.

Unlike other classes of flows, such as airfoils and forebodies, a straightforward use of grid stretching does not yield accurate results in the presence of massive separation. Reference 3 has implemented grid adaptation to better resolve the complex flow pattern, and reasonable (qualitative) agreement with a ground-based test experiment on an aerobrake configuration (AFE) has been obtained by an adaptive clustering of mesh points in the afterbody where large gradients occur. Reference 3 also reports the occurrence of some instability at the wake neck. By assuming a constant Strouhal number of 0.3 and using the wake neck thickness as the characteristic length scale, it is shown that wake instability frequencies can be well predicted, yielding results consistent with experimental data.[3] More importantly, it is concluded that, on account of the freezing of the flow in the base region, the latter can be well analyzed by means of an ideal-gas model. In Ref. 15 the effects of the angle of attack on the shear-layer angle has been investigated, showing that at low Reynolds number (corresponding to flow situations early in the reentry trajectory) the boundary layer separates at a greater distance from the shoulder and the shear layer is more likely to impinge on the afterbody surface. Under these circumstances the peak heating can be a significant fraction of the stagnation-point value. Reference 15 also shows that the formation of a reverse normal shock in front of the base stagnation point may occur, depending upon freestream conditions and geometry.

The present paper is aimed at investigating steady solutions, focusing on the characterization of the near-wake flows: detachment, free-shear-layer evolution, lip-shock generation, recirculation structure, and upstream influence. In particular, we have analyzed near-wake flows around both sharp- and blunt-nosed bodies (for both planar and axisymmetric configurations), all having sharp corners, for Reynolds numbers of $\sim 10^3$–10^6 and Mach numbers of ~ 10. The model employed is based on an ideal-gas assumption, whereby real-gas effects are neglected. The use of an ideal-gas model certainly contributes to the understanding of the physics of the near wake, which is basically a fluid-dynamic phenomenon (the assumption is justified on recalling that in the hypersonic case the nonequilibrium effects dominate the forebody region, while the afterbody flow is nearly frozen[3,13,14]; however, the expansion in the base may depend on the value of the specific heat ratio). It is important to observe that, due to model uncertainties and computer limitations, a complete model allowing for chemical and thermal relaxation processes, turbulence, and unsteadiness, as well as radiation, ablation, and catalytic wall effects, is still unrealistic. For example, a typical three-dimensional nonequilibrium base-flow computation[14] requires (on a grid that is too coarse to resolve the fine detail of separation and upstream influence) about 50 h of CPU time on a Cray-2. In the following sections, we briefly describe the numerical solution; then we extensively discuss the results and give some concluding remarks.

Numerical Solution

The objective of this work is the characterization of the mechanism of upstream influence and the structure of the near wake. Because of the complexity of these phenomena, the full laminar compressible Navier–Stokes equations in their conservation form are solved. These are discretized by a finite-volume approach in order to reduce the system of conservation equations to the following semidiscrete form[16]:

$$V\frac{\mathrm{d}\boldsymbol{W}}{\mathrm{d}t} + \boldsymbol{R} = \boldsymbol{0} \tag{1}$$

where $\boldsymbol{W} = [\rho, \rho\boldsymbol{u}, \rho E]^T$ is the vector of conservative unknowns, which are assumed to be piecewise constant within each finite volume V, and the residual $\boldsymbol{R}$ allows for the approximation of the inviscid and viscous flux contributions.

For the discretization of the inviscid flux we have employed a second-order upwind-biased total-variation-diminishing scheme, originally developed in Refs. 17–19 and extensively used and validated for hypersonic applications.[16,20] The numerical approximation of space derivatives needed for evaluating the viscous contribution is obtained from second-order discretization formulas by means of the Gauss theorem. The time integration of the equations is performed by means of a multistage Runge–Kutta algorithm with coefficients optimized for damping high-frequency errors.

A subdomain approach has been employed to accurately resolve the base-flow region: an outer subdomain has been used for the forebody and the downstream outer region, and the second subdomain corresponds to the wake region. A typical arrangement is shown in Fig. 3a, where the body contour, the outer computational boundary, and the interface between the two blocks are depicted. A critical requirement arising with a multiblock approach is for a correct treatment of block interfaces to avoid a loss of accuracy and robustness of the numerical scheme. The problem has been solved by a conservative treatment of the interface fluxes and by injection of the conservative variables from one block to the other.[21] The grid has been generated with an appropriate clustering of mesh points to accurately resolve the boundary layer and the shear layer. Obviously, this procedure may lead to undesired high grid densities even in regions of smooth properties. As discussed in the introduction, we are only interested in steady-state solutions at zero angle of attack.

Results

The objective of the present work is a characterization of near-wake flows in terms of upstream influence, separation location, aspect ratio of the wake (defined as the ratio of the wake neck thickness to the recirculation length), compressibility effects in the wake, and character of the recirculation wake structure. With regard to the latter point, we are mainly concerned with identifying the conditions under which the wake is convection-dominated (i.e., the recirculation wake shows an inviscid core with nearly constant vorticity or diffusion-dominated (i.e., with a varying-vorticity core). For validation purposes, we first computed two test cases for a planar and axisymmetric configuration to assess the quality of the predicted results.

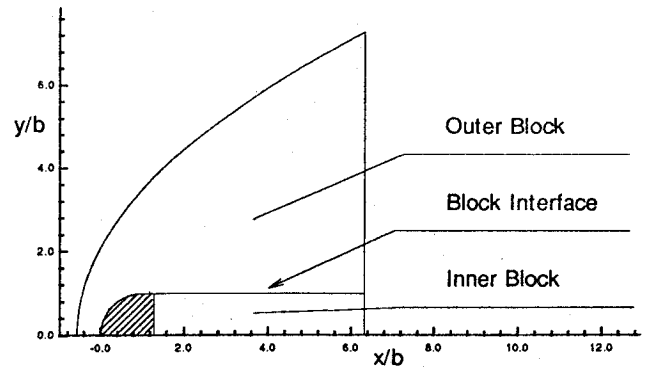

a) G-1: cylinder–slab (planar), sphere–cylinder (axisymmetric)

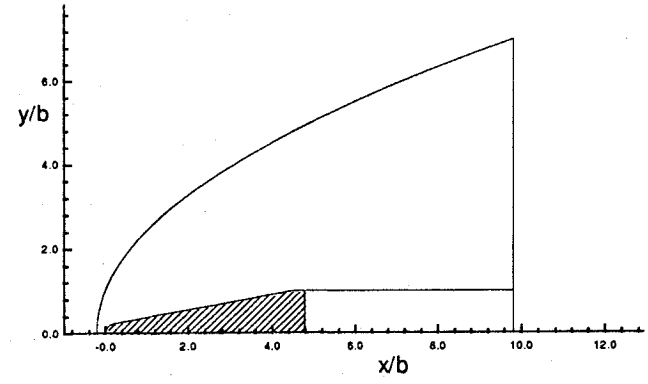

b) G-3: blunted wedge–slab (planar), blunted cone–cylinder (axisymmetric)

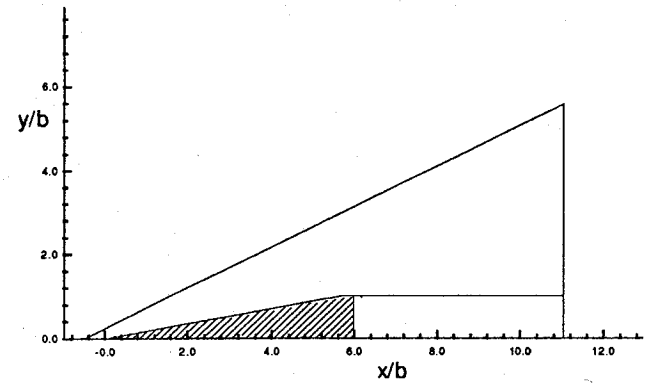

c) G-2: wedge–slab (planar), sharp cone–cylinder (axisymmetric)

Fig. 3 Test geometries and computational domains.

Validation Study

The first validation test case was selected from the experimental investigation[22] of the laminar near wakes behind a 10-deg-half-angle wedge at $M_\infty = 6$. The conditions correspond to a cold wall with $T_w/T_{0,\infty} = 0.19$ and unit Reynolds number $Re/\mathrm{m} = 1.85 \times 10^6/\mathrm{m}$. For comparison purposes in Fig. 4, we report the flowfield in terms of streamlines and stagnation temperature. It is interesting to observe that the latter exhibits minor variations along the streamlines, but only outside the base-region shock boundaries (determined by the lip and recompression shocks). The figure shows that the computation reproduces accurately the bow and embedded shocks, as well as the streamline pattern. Qualitatively the computed stagnation temperature shows no appreciable differences from the measured values. At

Table 1 Test-case conditions and characteristic quantities[a]

Test	Geom.	L/b	Re_∞	M_∞	Re_{sh}		M_{sh}		δ_s		Re_{ds}		ω_w	
					P	A	P	A	P	A	P	A	P	A
1	G-1	1.3	2,250	11.6	340	400	2.0	2.7	2.7	2.5	37	19	160	165
2	G-1	1.3	22,500	11.6	2,700	2,200	2.3	2.8	0.9	0.95	500	380	450	420
3	G-1	1.3	225,000	11.6	24,000	21,200	2.3	2.8	0.3	0.33	4,500	3,500	1,350	1,200
4	G-1	1.3	22,500	15.0	2,200	1,700	2.3	2.81	0.85	0.87	400	300	650	610
5	G-1	1.3	22,500	8.0	4,000	3,300	2.2	2.73	1.07	1.14	630	490	270	255
6	G-2	5.97	22,500	11.6	33,000	38,100	7.0	7.7	1.2	0.97	75	82	300	360
7	G-3	4.78	22,500	11.6	2,500	31,300	2.5	8.0	1.5	1.31	230	110	270	305

[a]P = planar; A = axisymmetric.

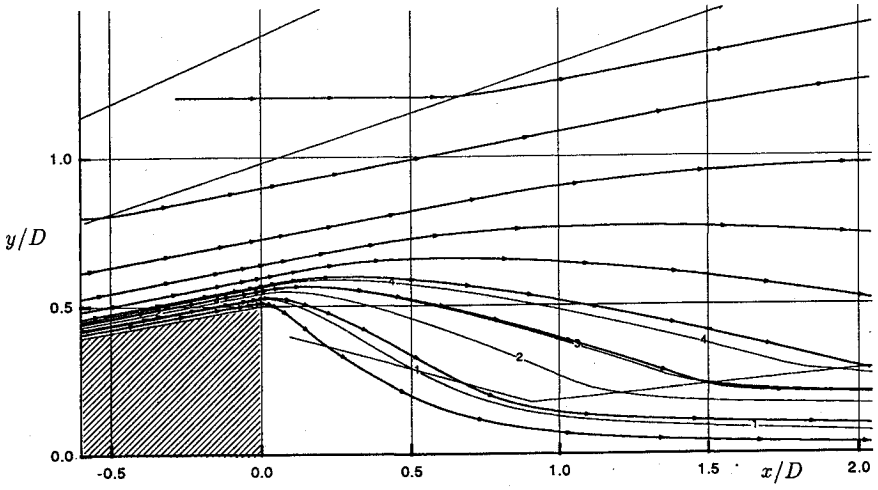

a) — $T/T_{0,\infty}$ computed

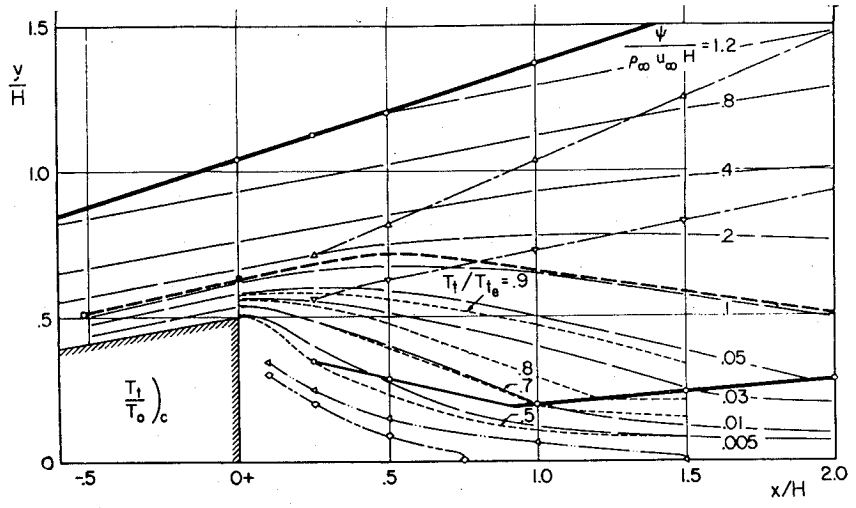

b) - - - $T/T_{0,\infty}$ (from Ref. 23, copyright © 1968, AIAA; reprinted with permission)

Fig. 4 Near-wake flowfield behind a 20-deg cold-wall wedge at $Re_b = 7.12 \times 10^3$ ($T_w T_0 = 0.19$).

the rear stagnation point, the computed value of the stagnation temperature (normalized by the freestream) on the axis is 0.32, whereas the measured one is 0.34.

The second validation test corresponds to the near-wake flowfield measurements[6] behind a 10-deg-half-angle cone at $M_\infty = 16$. The selected conditions correspond to a cold wall with $T_w/T_{0,\infty} = 0.125$ and $Re/\text{m} = 1.74 \times 10^4/\text{m}$. The computed centerline stagnation temperature in the wake is reported in Fig. 5a, and it shows good agreement between the computations and the experiments. The comparison of transverse stagnation-temperature profiles in the wake at two locations ($x/b = 1.2$ and 3.5) is reported in Fig. 5b, and it again shows good agreement between the simulations and the experiments.

Parametric Study

A parametric study was then performed to assess the effects of nose bluntness, and Mach and Reynolds numbers (the latter based on the half base height b, with $b = 0.038$ m for all test cases), whose values are given in Table 1. For all tests, a freestream temperature of $T_\infty = 122$ K, and cold-wall condition with $T_w = 294$ K, has been used. Base flows have been simulated for the geometries shown in Fig. 3 for both the planar (P) and axisymmetric (A) configurations, and some (computed) characteristic quantities are reported in Table 1.

For the most severe test case, corresponding to the highest Reynolds number (test case 3), a limited grid sensitivity study has been performed by varying the total number of mesh cells by halving and doubling the number of mesh points in both directions ($N =$ 8,000, 32,000, 128,000). The study shows that the separation location is the most sensitive quantity to the mesh resolution. For most of the calculations, a grid having about 20,000 cells in the outer domain and about 10,000 cells in the wake block has been used, with about 10–20 cells along the base between the corner and the separation point to properly resolve the fast flow turn at the shoulder.

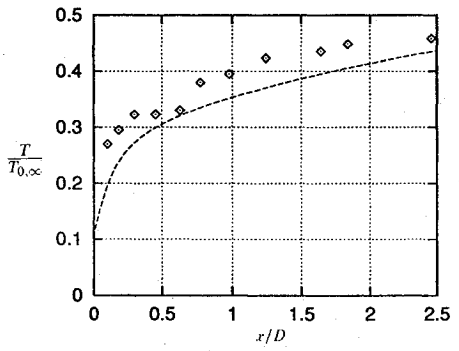

a) Along wake centerline: ◇, Ref. 6; dashed curve, computed

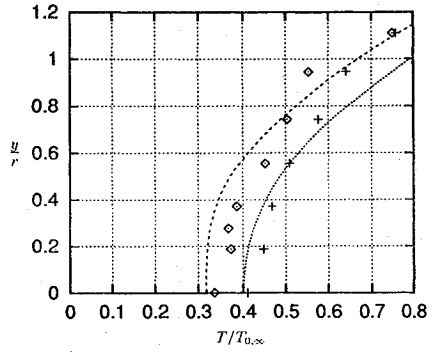

b) Along wake sections: ◇, at $x/D = 0.609$; +, at $x/D = 1.750$ (from Ref. 6); dashed and dotted curves, computed

Fig. 5 Stagnation temperatures in the wake: comparison between present computation and experiment.

We estimate an accuracy of about 20% in the computed upstream influence and near-wake extent.

Vorticity distributions in the recirculation core and near-wake streamlines computed for the various cases are reported in Figs. 6 and 7, respectively. For the understanding of near-wake flows, it is important to determine some basic quantities to which base flow properties are to be referred. Mach and Reynolds numbers cannot be used for characterizing the near-wake structure, since they do not allow for the effects of different forebody geometries. In principle, base flowfields depend on the flow properties measured at some distance upstream of the shoulder, just before the expansion begins. We expect the boundary-layer structure to play the most important role in the evolution of base flows, in particular the wall vorticity evaluated just before the shoulder.

The importance of wall vorticity has been recognized by several authors. In particular, Leal[23] has analyzed vorticity transport in the incompressible wake of bluff bodies at high Reynolds number, and has shown that the key point in the generation of the wake is the balance between convection and diffusion of the vorticity generated at solid surfaces. He examined the effects of the Reynolds number and concluded that recirculation wakes of finite extent exist at high Re due to the increase of both wall vorticity and convection. The analysis in Ref. 23 is limited to incompressible flows. Obviously, under hypersonic conditions compressibility effects cannot be disregarded (indeed, our calculations show that the Mach number in the recirculation wake grows with Re). In fact, recalling that wall vorticity is related to the skin-friction coefficient through the relation $\tau = \mu\omega_w$, one obtains

$$\omega_w = C_f\, Re_\infty\, M_\infty f(\gamma, T_\infty, T_w) \qquad (2)$$

thus establishing that the Mach number also contributes to the accumulation of vorticity in the recirculation wake.

However, the characteristic properties of the boundary layer (at the shoulder) alone cannot account simultaneously for all effects including the geometry effects. Let us consider for example test cases 6 and 5 (planar configuration) of Table 1, which differ in both geometry and freestream Mach number. From the values reported in the table, we observe that the wall vorticity evaluated

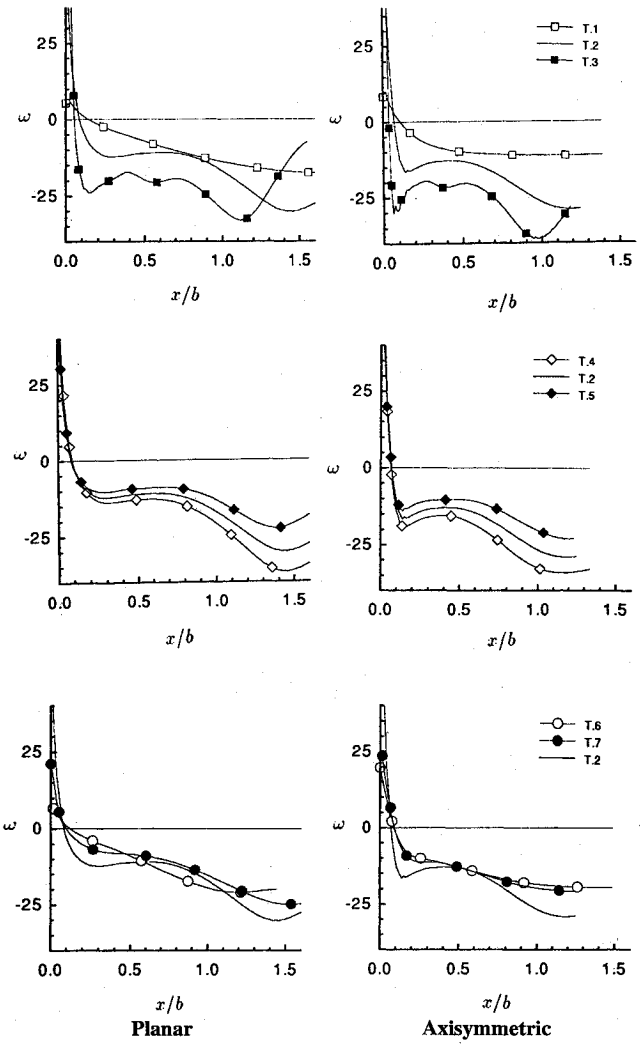

Fig. 6 Vorticity distribution in recirculation core; $T \cdot n$, test case n.

in the proximity of the corner is approximately equal in the two cases. Nonetheless, the flow features of the two test cases are different. Indeed, looking at the vorticity distribution in the recirculation wake reported in Fig. 6, we observe that test case 5 has a nearly constant-vorticity core (of extent approximately equal to the half base height b), whereas no such constant-vorticity core is present in test case 6. On the other hand, if we consider test cases 6 and 1, which differ in geometry and freestream Reynolds number, we observe that to comparable values of the near-corner wall vorticity correspond qualitatively similar flow features: both cases indeed show diffusion- rather than convection-dominated behavior, as observed from Fig. 6.

The above considerations lead us to conclude that the important parameters are not only the boundary-layer properties in the proximity of the corner, but also the properties in the near wake, mainly along the dividing streamline (i.e., the streamline that separates the outer region from the inner recirculation core), and in particular the dividing-streamline Reynolds number. The above statement can be justified by observing that the streamlines closest to the surface are the ones that undergo the separation process, and they are the ones closest to the dividing streamline. The role played by the latter is very important, since it is across this line that energy and momentum transfers occur, thus allowing the recirculation zone to form.

The importance of the dividing-streamline Reynolds number has been recognized by others. Weiss,[9] for example, has shown the influence of Re_{ds} on the vorticity and temperature fields, and observes that at $Re_{ds} \sim 300$ the near-wake structure has a constant-vorticity core, and it is controlled both by the base-wall boundary layer and the shear layer that develops along the dividing streamline. The occurrence of a constant-vorticity core in recirculation wakes at high Reynolds numbers has also been shown.[24] Thus, we can state

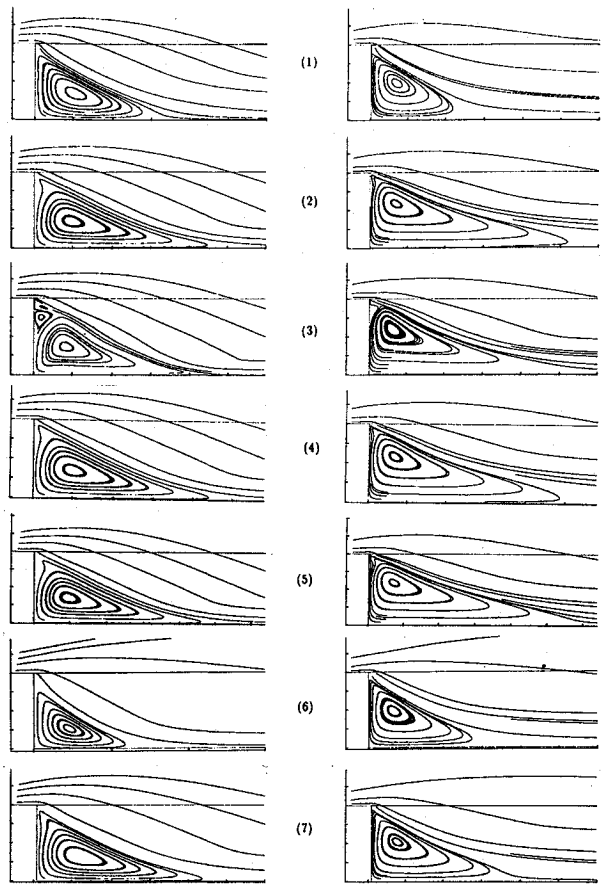

Fig. 7 Near-wake streamlines (test-case numbers in parentheses).

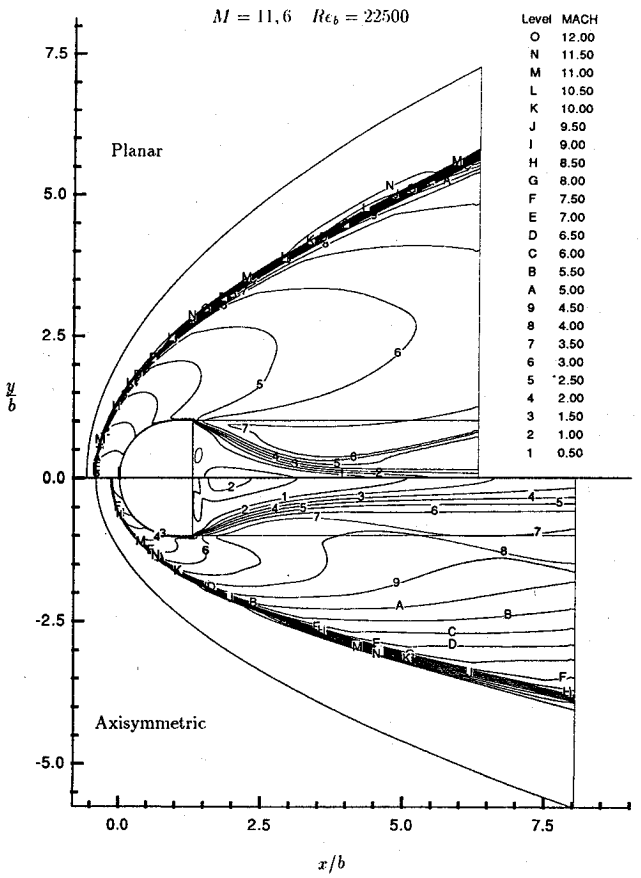

Fig. 8 Mach-number distribution for test case 2.

that near-corner quantities such as the Mach and Reynolds numbers, wall vorticity, and boundary-layer thickness, together with the dividing-streamline Reynolds number, are quantities that characterize the upstream influence, the separation location, and the evolution of the near wake.

Flow Structure

We now describe qualitatively the influence of the geometry and the Mach and Reynolds numbers on the near-wake flow structure. The iso-Mach lines for test case 2 (both planar and axisymmetric) of Table 1, depicted in Fig. 8, bring out the typical flowfield features described in the introduction. Note that, in the axisymmetric configuration, the squeezing of the flow is responsible for 1) the thinner shock layer and reduction of standoff distance, 2) the thicker near wake, and 3) the larger afterbody Mach number.

Reynolds-Number Effects

The effects of the Reynolds number have been studied for the geometry G-1 of Fig. 3, and the flow conditions correspond to those of test cases 1, 2, 3 of Table 1. In general, the forebody is responsible for the production of vorticity, which is then convected downstream and diffused across the dividing streamline toward the base with the establishment of a recirculation region. As the Reynolds number increases, the viscous dissipation effects are confined to thinner regions, and the free shear layer, the wake neck, and the wake trail all tend to be smaller. From the vorticity and streamline distributions in the near-wake core shown in Figs. 6 and 7, we observe a dramatic change in the near-wake structure as Re increases: 1) the near wake is diffusion-controlled at low Re, and convection-dominated at high Re; and 2) a secondary recirculation appears at the highest Reynolds number. The secondary recirculation is clearly detected immediately past the lip shock and is the consequence of an increase in the wall production of vorticity along the base (due to the boundary-layer development along the base itself), and it can be interpreted as an accumulation of opposite-sign vorticity on the base wall. An investigation of the vorticity distribution within the secondary recirculation (presented in Fig. 9) indicates that the latter has a constant-vorticity core.

To understand the mechanisms of energy and momentum exchanges between the recirculation region and the outer flow, we have also analyzed the evolution of vorticity, whose transport equation is

$$\frac{D\omega}{Dt} = \underbrace{-\omega\nabla\cdot\boldsymbol{u}}_{(C)} + \underbrace{\omega\cdot\nabla\boldsymbol{u}}_{(VS)} + \underbrace{\frac{1}{\rho^2}\nabla\rho\times\nabla p}_{(B)} - \underbrace{\frac{1}{\rho^2}\nabla\rho\times(\nabla\cdot\sigma)}_{(CV)}$$

$$+ \underbrace{\frac{1}{\rho}\mu\nabla^2\omega}_{(D)} + \underbrace{\frac{1}{\rho}\nabla\mu\times[\nabla^2\boldsymbol{u}+\nabla(\nabla\cdot\boldsymbol{u})]}_{(VV)} \qquad (3)$$

where the meaning of the different terms is as follows: C is vorticity production due to compressibility; VS is the vortex stretching, which is nonzero for the axisymmetric case (being equal to $\omega v/r$); B is the baroclinic contribution; CV represents the compressibility–viscosity interaction; D is the diffusion transport; and VV is a mixed production due to viscosity–velocity gradients. From the numerical simulations, we have found that the leading contributions (whose distributions are not reported) are the compressibility, diffusion, and baroclinic terms (the latter being generally smaller by a factor of 5). The outer flow releases vorticity to the main eddy along the dividing streamline, mainly through diffusion, whose contribution is very large just after separation but tends to die out rapidly downstream. Within the recirculation core, the diffusion contribution becomes more and more negligible as the Reynolds number increases. Around the corner, the flow expansion acts [mainly through term C of Eq. (3)] as a vorticity reduction mechanism (a sink), whose strength increases with the Reynolds number. On the other hand, the recompression, which follows the overexpansion (and which at high Re turns into the lip shock), acts as a vorticity production mechanism, mainly through terms C and B of Eq. (3). In general, a core structure of alternating vorticity reduction and vorticity production has been observed in the near wake, as sketched in Fig. 10.

Mach-Number Effects

The influence of the Mach number on the near-wake structure has been studied for the blunted geometry G-1 of Fig. 3. The

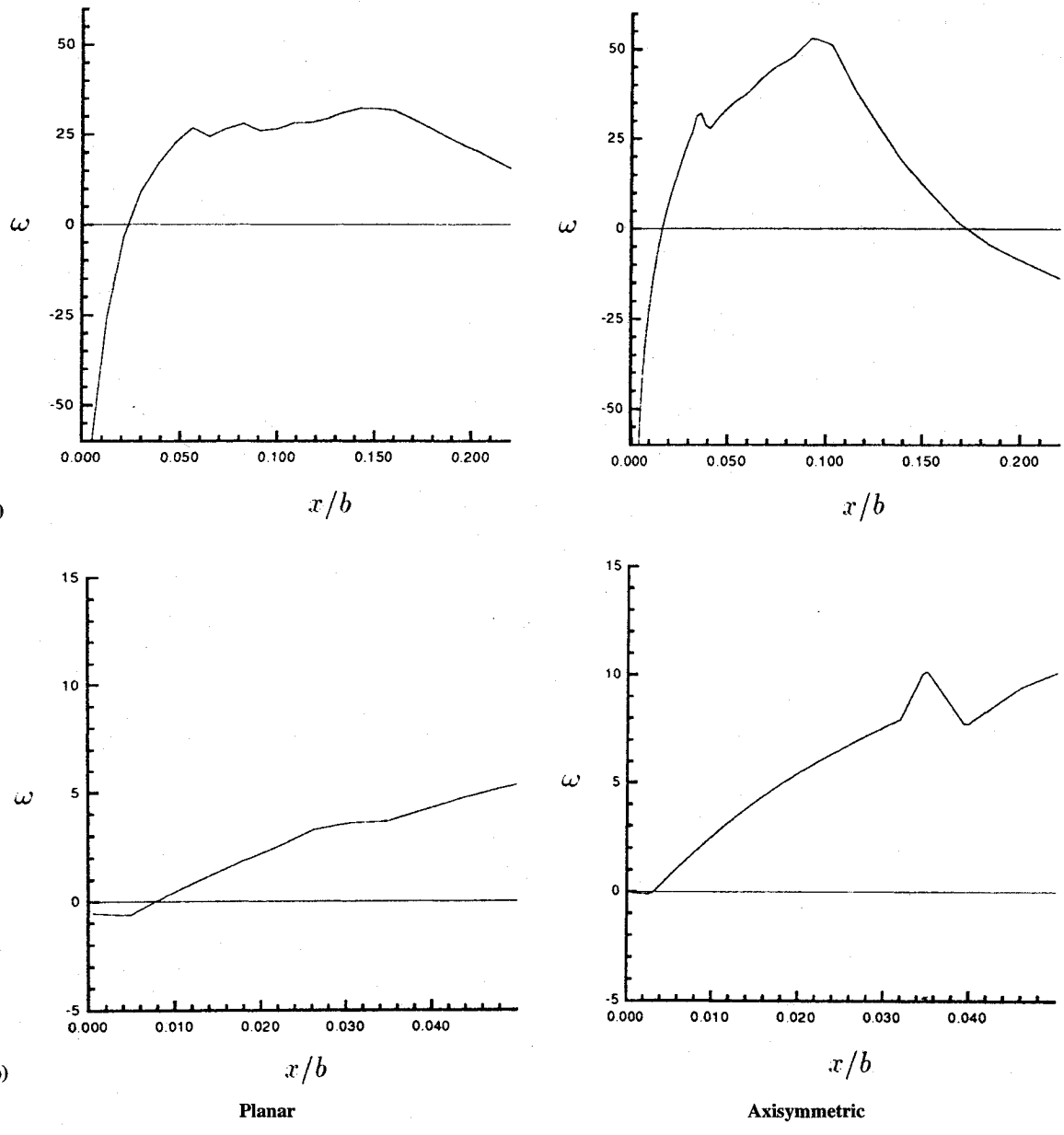

Fig. 9 Vorticity distribution in secondary recirculation: a) test case 3, and b) test case 5.

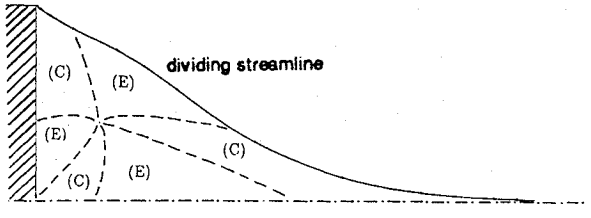

Fig. 10 Sketch of compressibility effects in the recirculation region: (C) compression; (E) expansion.

test conditions correspond to those of test cases 2, 4, and 5 of Table 1.

From the near-wake streamlines and vorticity distributions we observe a substantial change in the structure of the recirculation wake with the Mach number. The wake changes from diffusion- to convectionlike as the Mach number decreases, with the formation of a (small) secondary recirculation at $M_\infty = 8$. However, as observed in Fig. 9, this secondary recirculation does not exhibit a constant-vorticity core; instead, it shows a vorticity distribution typical of a diffusion-dominated recirculation. The change in wake behavior with Mach number can again be explained in light of the dependence of the leading contributions to the vorticity transport. Recall that for a blunt geometry, assuming the hypersonic limit ($M_\infty \to \infty$), the Reynolds number in the shock layer is $O(1/M_\infty)$. As a consequence, the ratio of diffusion to convection vorticity contributions increases with Mach number, thus explaining the convective near-wake behavior for the low-Mach-number case.

Geometry Effects

The influence of the geometry has been studied for given freestream Mach and Reynolds numbers, with the aim of investigating the effects of the rotationality induced by the (forebody) nose bluntness (the latter being measured in terms of the ratio of nose radius to half base height, R_N/b). In particular, we have considered the values $R_N/b = 0$, 0.025, and 1, corresponding, respectively, to test cases 6, 7, 2 of Table 1.

From the computed results we observe that nose bluntness modifies the geometrical features of the recirculation wake: the more blunt the nose, the more elongated and the more convective the wake is. Indeed, nose bluntness produces a detached curved bow shock that contributes to the vorticity production. From Fig. 6 we observe the change in the vorticity distribution in the recirculation core from diffusion- to convectionlike as R_N/b increases: the extent

of the constant-vorticity core is about 50% of the half base height for $R_N/b = 1$.

Scaling Laws

In this subsection, an attempt is made to establish scaling laws for the characteristic quantities that affect the near-wake flow behavior. First of all, we recall that the expansion around the shoulder plays an important role in the establishment of the dividing streamline and in the lip-shock formation.[11] This point is also supported by experimental evidence that indicates that the dynamics of the expansion is largely controlled by an inviscid pressure mechanism.

Hence, if one assumes a Prandtl–Meyer expansion around the shoulder, one can show that the dividing-streamline Reynolds number can be correlated with flowfield properties at the edge of the forebody boundary layer at the shoulder (more precisely, at the location of upstream influence). The functional dependence of Re_{ds} can then be determined in terms of postexpansion properties, even though the role of the boundary layer and the upstream influence is completely neglected when using a Prandtl–Meyer model. It is trivial to show that, employing the Chapman–Rubesin approximation for the viscosity law ($\mu \propto T^{\alpha}$), one obtains

$$Re_{ds} = \frac{\rho_{ds} u_{ds} b}{\mu_{ds}} = Re_{sh} \frac{\rho_{ds}}{\rho_{sh}} \frac{u_{ds}}{u_{sh}} \left(\frac{T_{ds}}{T_{sh}} \right)^{\alpha} \tag{4}$$

If one assumes for the density, velocity, and temperature ratios the hypersonic-limit ($M_{\infty} \to \infty$) expressions for the Prandtl–Meyer relations (for a dividing-streamline angle of about 30 deg), then the following holds:

$$Re_{ds} = Re_{sh} M_{sh}^{-\beta_r} \tag{5}$$

where $\beta_r = 2/(\gamma - 1) - 2\alpha$; with $\alpha = \frac{3}{4}$ (and $\gamma = \frac{7}{5}$) one gets $\beta_r \sim 3.5$.

It is interesting to observe that for all test cases (either planar or axisymmetric) the same power-law dependence ($Re_{ds} \propto Re_{sh}^{\alpha_r} M_{sh}^{-\beta_r}$) is numerically recovered, as Fig. 11 shows; in particular, the computations yield

$$Re_{ds} \propto Re_{sh}^{1.25} M_{sh}^{-\beta_r} \tag{6}$$

where for the planar (axisymmetric) configuration $\beta_r \sim 4.3$ (~3.8). The above expression shows that 1) the greater the Mach number at the edge of the shoulder boundary layer, the lower the dividing-streamline Reynolds number, and 2) the higher the Reynolds number, the higher the dividing-streamline Reynolds number.

We are now in a position to characterize the behavior of the near wake, mainly in terms of Re_{ds}. The obtained results are summarized in Table 2.

Upstream Influence

To characterize the near-wake influence, it is important to determine the extent of the upstream influence of the expansion around the corner (i.e., the influence of the afterbody on the forebody flowfield). It must be pointed out that in the supersonic portion of the boundary layer the expansion is controlled by the curvature of the sonic line, whereas the low-pressure signals propagate upstream through the subsonic portion of the boundary layer. In Fig. 12a, the tangential velocity gradient is reported vs the normal distance from the wall at different locations from the corner ($\Delta s/b = 0$). The figure clearly shows that it is the near-wall vorticity ($\omega \approx du/dy$) that is mainly affected by the upstream influence, and the effects are negligible outside the subsonic portion of the boundary layer. Then, to establish a functional dependence of the upstream influence length $\Delta\ell$ one may apply the boundary-layer equations in the proximity of the wall.[25] By so doing the pressure drop, which occurs over a distance of order $\Delta\ell$, can be related to the skin friction and to the subsonic boundary-layer thickness δ_s evaluated at the section immediately before the extent of upstream influence, i.e.,

$$\frac{\Delta\ell}{\delta_s} \propto \frac{\Delta p/p}{C_f} \tag{7}$$

The above relation shows a dependence of $\Delta\ell$ on the expansion around the corner and the Reynolds number. Hence, recalling that

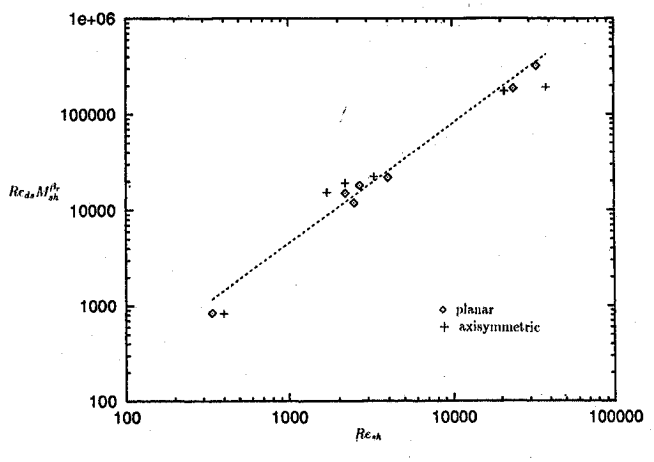

Fig. 11 Dividing-streamline maximum-Reynolds-number distribution for all test cases.

Table 2 Near-wake behavior

$Re_{ds} \leq 100$	Diffusionlike behavior.
$100 < Re_{ds} \leq 500$	The recirculation wake changes from diffusion- to convectionlike, showing a constant-vorticity core whose extent increases with Re_{ds}.
$500 < Re_{ds} \leq 1000$	Convectionlike behavior, with the presence of a secondary recirculation that does not present a constant-vorticity core.
$Re_{ds} > 1000$	Convectionlike behavior, with a secondary recirculation that shows a constant-vorticity core.

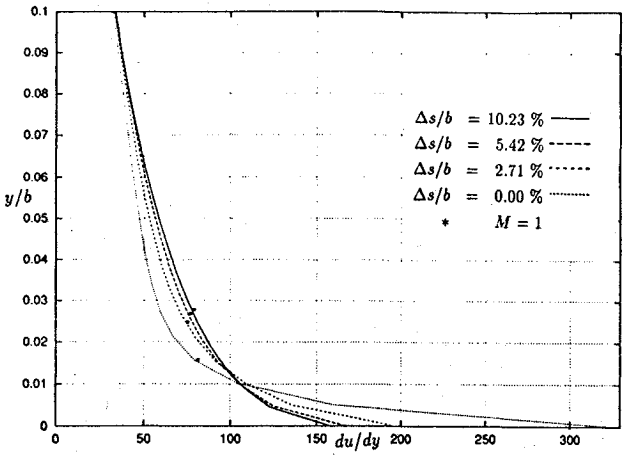

Fig. 12a Distribution of du/dy normal to the wall at various distances from the corner.

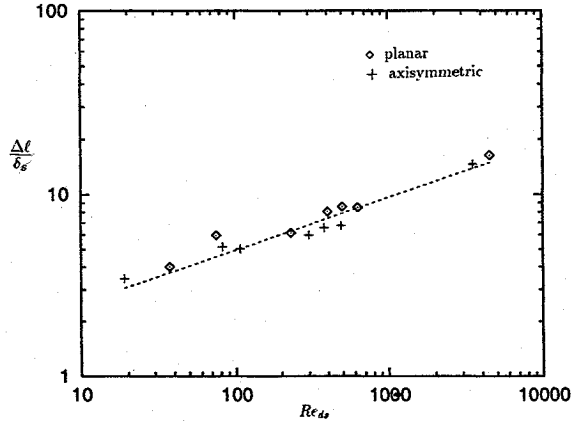

Fig. 12b Upstream influence vs Re_{ds}.

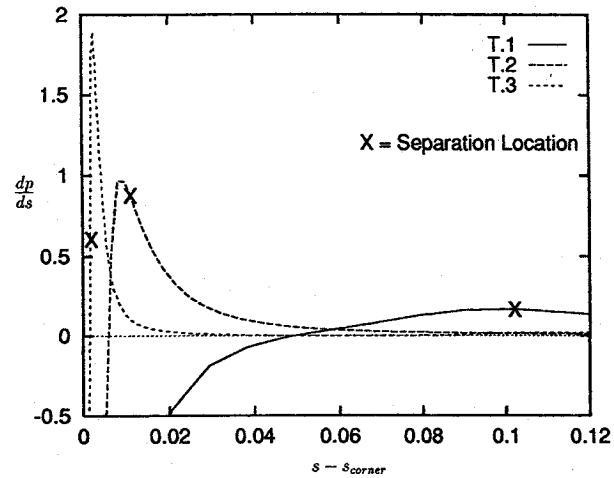

Fig. 13a Distribution of dp/ds along the base wall.

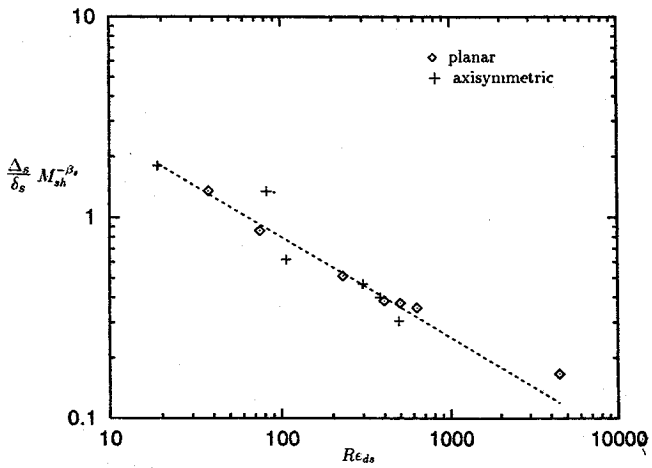

Fig. 13b Separation distance from corner vs Re_{ds}.

Re_{ds} does indeed depend on the corner expansion and Re, we reason that

$$\frac{\Delta \ell}{\delta_s} \propto Re_{ds}^{\alpha_i} \tag{8}$$

and from the computed results reported in Fig. 12b we obtain for both the planar and axisymmetric configurations $\alpha_i \sim \frac{1}{3}$.

Separation Location

With regard to separation, it must be observed that, because of the favorable streamwise pressure gradient along the wall, the flow turns around the shoulder, separating at a distance from the corner immediately before the recompression that follows the overexpansion. In particular, it is observed that separation is strictly related to the occurrence of a local peak in the pressure gradient (dp/ds) along the base, as Fig. 13a shows, where the distribution of dp/ds is reported vs the distance from the corner along the base.

To characterize simultaneously the influence of geometry and Mach and Reynolds numbers on the separation, it is useful to recall that, according to the findings of Ref. 10, the separation point moves away from the corner as the Reynolds number decreases. Moreover, Ref. 11 has also argued that there may be an inviscid wave interaction mechanism that strengthens the lip shock, thus affecting the separation. We then reason that the separation location depends on Re_{ds} and M_{sh} (where the latter is assumed to characterize the strength of the interaction mechanism), i.e.,

$$\frac{\Delta s}{L} \propto Re_{ds}^{\alpha_s} M_{sh}^{\beta_s} \tag{9}$$

where L is a reference length. Recalling that pressure signals propagate upstream through the subsonic portion of the boundary layer, it is again reasonable to choose as reference length the thickness of the subsonic boundary layer at the shoulder. Then, for all test cases,

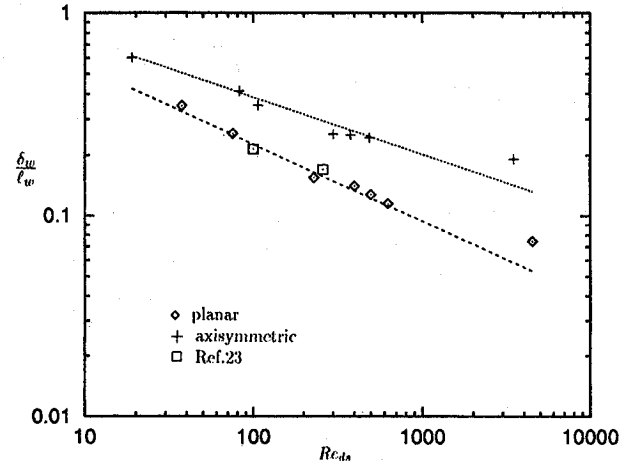

Fig. 14 Wake neck thickness vs Re_{ds}.

the separation location Δs, measured with respect to the corner, is found to obey the following scaling law:

$$\frac{\Delta s}{\delta_s} \propto Re_{ds}^{\alpha_s} M_{sh}^{\beta_s} \tag{10}$$

where $\alpha_s \sim -\frac{1}{3}$ and $\beta_s \sim 1.4$ (~0.9) in the planar (axisymmetric) configuration, as inferred from Fig. 13b.

Near-Wake Aspect Ratio

Two important parameters that characterize the extent of the near-wake region are the recirculation extent l_w, defined as the distance of the rearward stagnation point from the base wall along the wake axis, and the wake neck thickness δ_w, defined as the minimum wake thickness. First of all we recall that for a given (cylindrical) geometry and (hypersonic) Mach number, Ref. 2 shows that δ_w correlates with the boundary-layer thickness at the shoulder (δ_{sh}), i.e., $\delta_w \propto Re_\infty^{-1/2}$. With regard to the extent of the recirculation wake (for a fixed geometry and Mach number), from Table 1 we observe that ℓ_w at first increases with the Reynolds number, and then it approaches a value that is nearly independent of Re, in agreement with theoretical and experimental findings that show finite recirculation extent at very high Reynolds numbers. Moreover, we find that the wake neck thickness scales with the recirculation length and depends on the dividing-streamline Reynolds number according to the following law:

$$\frac{\delta_w}{\ell_w} \propto Re_{ds}^{\alpha_w} \tag{11}$$

where $\alpha_w \sim -\frac{1}{3}(-0.3)$ for the planar (axisymmetric) configuration. The above relation shows that Re_{ds} not only characterizes the internal structure of the recirculation(s), but also governs the aspect ratio (defined as δ_w/ℓ_w) of the near-wake region.

Figure 14 shows that indeed the above relation accounts simultaneously for geometry, and for Mach and Reynolds numbers. In the figure, we have also reported the values of the wake aspect ratio extrapolated from the experiments[22] at two Reynolds numbers ($Re/\mathrm{m} = 1.85 \times 10^6, 3.7 \times 10^6/\mathrm{m}$) corresponding to laminar cold-wall conditions. For these cases, we have determined the dividing-streamline Reynolds number by extrapolating the shoulder conditions from the measurements[22] and using the correlation corresponding to Eq. (6). The good agreement between the computed and measured results confirms the correlation between the wake neck thickness and the recirculation length.

For $Re_{ds} \geq 1000$ the results show a change in the value of the exponent α_w. It is interesting to observe that if one substitutes the scaling law for Re_{ds} [see Eq. (6)] in Eq. (11), one obtains $\delta_w/\ell_w \propto Re_{sh}^{-1/2}$. Hence, since the recirculation extent at high Reynolds conditions is nearly independent of Re, the same Reynolds-number scaling of δ_w is found.[2]

Compressibility Effects

To fully characterize the near wake it is also useful to evaluate the importance of compressibility in terms of characteristic Mach

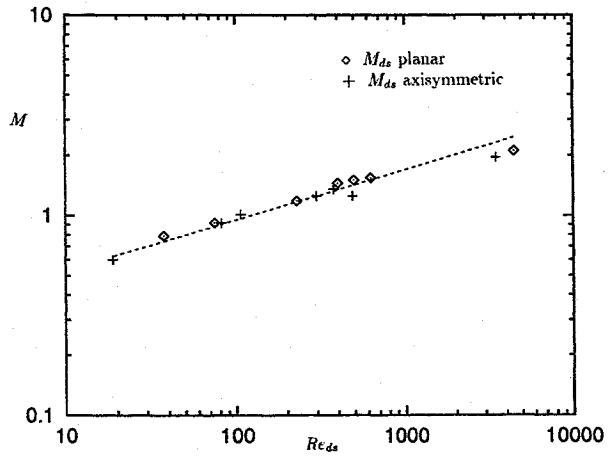

Fig. 15a Dividing-streamline Mach-number distribution.

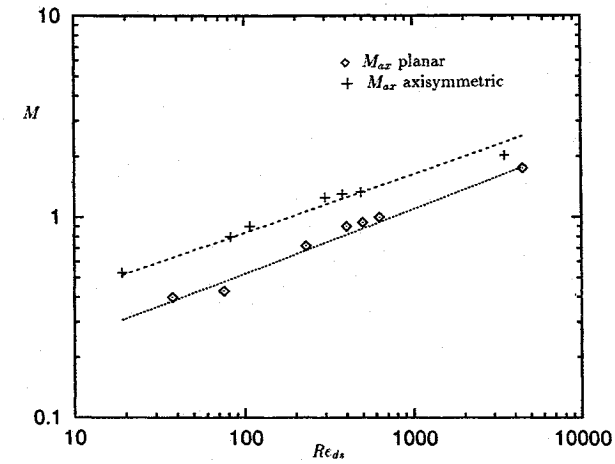

Fig. 15b Centerline Mach-number distribution.

numbers in the wake. For that purpose we have introduced two Mach numbers: the maximum Mach number along the dividing streamline ($M_{\rm ds}$) and the maximum one on the symmetry axis ($M_{\rm ax}$). From the analysis carried out in the present work we observe that the higher the Reynolds number, the higher the kinetic energy content of the near-wake recirculation and the higher the local Mach numbers are. In particular, as shown in Fig. 15, we find that $M_{\rm ds}$ and $M_{\rm ax}$ scale with $Re_{\rm ds}$ according to

$$M_{\rm ds} \propto Re_{\rm ds}^{\alpha_d}, \qquad M_{\rm ax} \propto Re_{\rm ds}^{\alpha_a} \tag{12}$$

where for the planar (axisymmetric) geometries $\alpha_d \sim \frac{1}{4}$ and $\alpha_a \sim \frac{1}{3}$ (0.3). Hence, the flow becomes supersonic as the flow approaches the base wall, with the formation of a reverse-flow shock in front of the base stagnation point depending on the value of the dividing-streamline Reynolds number: supersonic conditions appear in the near-wake region for $Re_{\rm ds} > 100$, and a reverse-flow shock forms, whose strength increases as the behavior of the recirculation wake changes from diffusion- to convectionlike.

Base Pressure

With regard to the effects of Mach and Reynolds numbers and of slenderness (defined as the ratio of body length to half base height) on the base pressure, the computed results indicate that the latter decreases with increasing Reynolds number and slenderness, whereas it increases with the Mach number. In general, we observe that as the recirculation wake becomes more inviscid, the base pressure level is lowered. The role played by the dividing-streamline Reynolds number in determining the importance of viscous effects in the near wake has been clearly highlighted. A dependence of the computed base pressure on $Re_{\rm ds}$ is expected: Fig. 16 shows indeed that the higher the $Re_{\rm ds}$ (i.e., the more inviscid the near wake) the lower the base pressure.

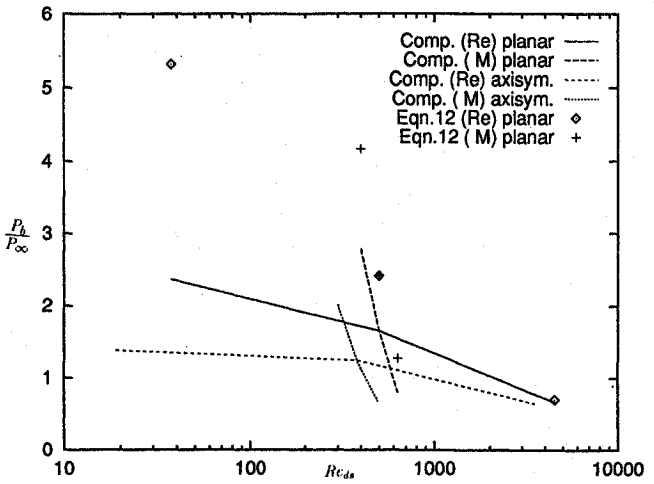

Fig. 16 Base pressure: comparison between computations and the Chapman model.

A (qualitative) confirmation of the dependence of p_b on $Re_{\rm ds}$ can be obtained by revisiting Chapman's constant-pressure mixing model.[1] Referring to Fig. 1, it is obvious that a particle along a streamline within the mixing layer will either flow downstream or remain trapped in the recirculation region, depending on the value of its total pressure: the particle will pass downstream if p_0 is greater than the pressure at reattachment. If one assumes 1) isentropic compression along the dividing streamline and 2) dividing-streamline total pressure constant and equal to the reattachment value, then the base pressure can be expressed according to

$$p_{0,\rm ds} = p_e\left(1 + [(\gamma - 1)/2]M_{\rm ds}^2\right)^{\gamma/(\gamma-1)}$$

where p_e is the pressure at the edge of the mixing layer. According to Chapman's constant-pressure mixing model, if we assume that p_e is constant and equal to the base pressure, we obtain

$$p_b = \frac{p_R}{\left(1 + [(\gamma - 1)/2]M_{\rm ds}^2\right)^{\gamma/(\gamma-1)}} \tag{13}$$

Obviously the above formula does not allow for the losses in the total pressure due to viscous effects; however, it shows that the base pressure correlates with the reattachment pressure and $M_{\rm ds}$. If one expresses $M_{\rm ds}$ in terms of the velocity ratio along the dividing streamline and the Mach number along the outer edge of the mixing layer, Eq. (13) (incorrectly) predicts a base pressure that is independent of the Reynolds number.[1] However, if one uses for $M_{\rm ds}$ the maximum value of the Mach number along the dividing streamline (which we recall, shows a power-law dependence on $Re_{\rm ds}$) and for p_R the computed pressure at reattachment, then the following dependence of the base pressure on the Reynolds and Mach numbers is recovered:

$$p_b = f(p_R, Re_{\rm sh}, M_{\rm sh}) \sim \frac{p_R}{\left(1 + A_p Re_{\rm sh}^a M_{\rm sh}^b\right)^{\gamma/(\gamma-1)}} \tag{14}$$

where

$$A_p = (\gamma - 1)/2, \qquad a = 2.5\alpha_d, \qquad b = -2\alpha_d\beta_r$$

The computed base pressure qualitatively agrees with the one evaluated with the formula given by Eq. (14), especially at high $Re_{\rm ds}$, as Fig. 16 shows.

Conclusions

In the present work, the influence of nose bluntness and of Mach and Reynolds numbers on the structure of hypersonic near wakes has been characterized. The study has clearly highlighted the effect of the flow properties on the dividing streamline, in particular the maximum value of the Reynolds number (defined as the dividing-streamline Reynolds number) as well as the properties at the edge of

the near-shoulder boundary layer. The structure of the recirculation region is diffusion-dominated for Re_{ds} below 100, and it changes from diffusion- to convectionlike, with the occurrence of a constant-vorticity core, for $Re_{ds} \geq 200$–300. When $Re_{ds} \geq 500$, secondary recirculations appear, and their character again depends on Re_{ds}. Some interesting scaling laws have been determined numerically and have been confirmed by theoretical considerations and experimental data on base flows. The upstream influence and the separation location scale with the thickness of the subsonic portion of the forebody boundary layer and Re_{ds}, whereas the near-wake thickness scales with the axial extent of the recirculation region and varies with Re_{ds}. Moreover, the compressibility effects in the near wake, measured in terms of the axial and dividing-streamline Mach numbers, are found to scale with Re_{ds}: supersonic conditions appear when the near wake is convection-dominated with the occurrence of a reverse-flow shock standing in front of the rear (base wall) stagnation point. Dependence of the base pressure on the dividing-streamline Reynolds number has been (qualitatively) proven by means of a simplified theoretical analysis based on a revised Chapman's constant-pressure mixing model.

References

[1]Berger, S. A., *Laminar Wakes*, 1st ed., American Elsevier, New York, 1971, pp. 37–40, 202–204.

[2]Dewey, C. F., Jr., "Near Wake of a Blunt Body at Hypersonic Speeds," *AIAA Journal*, Vol. 6, No. 3, 1965, pp. 1001–1010.

[3]Venkatapathy, E., Palmer, G., and Prabhu, D. K., "AFE Base Flow Computations," AIAA Paper 91-1372, June 1991.

[4]Kubota, T., and Dewey, C. F., Jr., "Momentum Integral Methods for the Laminar Free Shear Layer," *AIAA Journal*, Vol. 2, No. 4, 1964, pp. 625–629.

[5]McCarthy, J. F., and Kubota, T., "A Study of Wakes Behind a Circular Cylinder at $M = 5.7$," *AIAA Journal*, Vol. 2, No. 4, 1964, pp. 629–636.

[6]Todisco, A., and Pallone, A. J., "Near Wake Flow Field Measurements," *AIAA Journal*, Vol. 3, No. 11, 1965, pp. 2075–2080.

[7]Reeves, B. L., and Lees, L., "Theory of Laminar Near Wake of Blunt Bodies in Hypersonic Flow," *AIAA Journal*, Vol. 3, No. 11, 1965, pp. 2061–2074.

[8]Weiss, R. F., and Weinbaum, S., "Hypersonic Boundary-Layer Separation and the Base Flow Problem," *AIAA Journal*, Vol. 4, No. 8, 1966, pp. 1321–1330.

[9]Weiss, R. F., "Base Pressure of Slender Bodies in Laminar Hypersonic Flow," *AIAA Journal*, Vol. 4, No. 9, 1966, pp. 1557–1559.

[10]Hama, F. R., "Experimental Studies on the Lip Shock," *AIAA Journal*, Vol. 6, No. 2, 1968, pp. 212–219.

[11]Weinbaum, S., "Rapid Expansion of a Supersonic Boundary Layer and Its Application to the Near Wake," *AIAA Journal*, Vol. 4, No. 2, 1966, pp. 217–226.

[12]Allen, J. S., and Cheng, S. I., "Numerical Solution of the Compressible Navier–Stokes Equations for the Near Wake," *Physics of Fluids*, Vol. 13, No. 1, 1970, pp. 37–52.

[13]Candler, G., "The Computation of Weakly Ionized Hypersonic Flows in Thermochemical Nonequilibrium," Ph.D. Thesis, Stanford Univ., Palo Alto, CA, 1988.

[14]Palmer, G., "Explicit Thermochemical Nonequilibrium Algorithm Applied to Compute Three-Dimensional Aeroassist Flight Experiment Flowfields," *Journal of Spacecraft and Rockets*, Vol. 27, No. 5, 1990, pp. 545–553.

[15]Gnoffo, P. A., Price, J. M., and Braun, R. D., "On the Computation of Near Wake, Aerobrake Flowfields," AIAA Paper 91-1371, June 1991.

[16]Grasso, F., and Marini, M., "Solutions of Hypersonic Viscous Flows with Total Variation Diminishing Multigrid Techniques," *Computers and Fluids*, Vol. 23, No. 5, 1995, pp. 571–592.

[17]Harten, A., "High Resolution Schemes for Hyperbolic Conservation Laws," *Journal of Computational Physics*, Vol. 49, No. 3, 1983, pp. 357–393.

[18]Yee, H. C., Warming, R. F., and Harten, A., "Implicit TVD Schemes for Steady State Calculations," *Journal of Computational Physics*, Vol. 57, No. 3, 1985, pp. 327–360.

[19]Yee, H. C., Klopfer, G. H., and Montagńe, J. L., "High Resolution Shock Capturing Schemes for Inviscid and Viscous Hypersonic Flows," NASA TM 100097, April 1988.

[20]Grasso, F., and Capano, G., "Modeling of Ionizing Hypersonic Flows in Nonequilibrium," AIAA Paper 94-0763; also *Journal of Spacecraft and Rockets*, Vol. 32, No. 2, 1995, pp. 217–224.

[21]Quarteroni, A., "Domain Decomposition and Parallel Processing for the Numerical Solution of Partial Differential Equations," *Surveys on Mathematics for Industry*, Vol. 1, No. 1, 1991, pp. 75–118.

[22]Batt, R. G., and Kubota, T., "Experimental Investigation of Laminar Near Wakes Behind 20° Wedges at $M_\infty = 6$," *AIAA Journal*, Vol. 6, No. 11, 1968, pp. 2077–2083.

[23]Leal, L. G., "Vorticity Transport and Wake Structure for Bluff Bodies at Finite Reynolds Number," *Physics of Fluids A1*, Vol. 1, No. 1, 1989, pp. 124–131.

[24]Batchelor, G. K., "On Steady Laminar Flow with Closed Streamlines at Large Reynolds Number," *Journal of Fluid Mechanics*, Vol. 1, July 1956, pp. 177–190.

[25]Hayakawa, K., and Squire, L. C., "The Effect of the Upstream Boundary-Layer State on the Shock Integration at a Compression Corner," *Journal of Fluid Mechanics*, Vol. 122, Sept. 1982, pp. 369–394.

T. C. Lin
Associate Editor